Au-Mo-Fe-Ni/$CeO_2(Gd_2O_3)$ As Potential Fuel Electrodes For Internal CO_2 Reforming of CH_4 in Single SOFCs

E. Ioannidou, S. Neophytides, and D. K. Niakolas

Foundation for Research and Technology, Institute of Chemical Engineering Sciences (FORTH/ICEHT), Stadiou Str., 26504 Platani, Patras, Greece

In this study the catalytic and electro-catalytic performance, as well as the coking resistance of un-modified and modified Ni/$CeO_2(Gd_2O_3)$ with 3 wt.% Au−0.4 wt.% Mo and 3 wt.% Au−0.5 wt.% Fe electrocatalysts were studied as half and full electrolyte supported cells under internal CO_2 reforming of CH_4 in single SOFCs, at 750-900 ºC. The aim was to elucidate their activity towards the consumption of CH_4, CO_2, the production of H_2, H_2O, CO and the production of carbon, as a function of temperature and the applied current density under a biogas fuel mixture of CH_4/CO_2=1. Additionally, the cells comprising the electrocatalysts as fuel electrodes, 8 mol% Y_2O_3 stabilized ZrO_2 (8YSZ) as electrolyte and $La_{0.6}Sr_{0.4}Co_{0.8}Fe_{0.2}O_{3-\delta}$ (LSCoF) as oxygen electrode were characterized using I-V measurements and Electrochemical Impedance Spectra (EIS) analysis in order to investigate the evolution of the ohmic and polarization resistance values as a reflection of current.

Introduction

Recycling biogas to produce syngas (H_2 + CO) through Dry Reforming of Methane (DRM) has currently attracted resurgent interest. Biogas consists mainly of CH_4 (50-70%) and CO_2 (25-50%) and is widely produced by anaerobic fermentation of biomass (1). DRM provides a feasible solution to eliminate greenhouse gases via production of useful chemicals and hydrocarbons.

Considering the DRM energy applications the produced syngas can be used as a fuel in high temperature solid oxide fuel cells (SOFCs) for electricity production or biogas can be directly fueled in the cell without the need of an external reformer (Internal Dry Reforming of Methane, IDRM), which simplifies the SOFC system and reduces the cost (2,3). When biogas is directly fed to the SOFC fuel electrode at temperatures 750-900 ºC, various catalytic and electrocatalytic reactions may take place simultaneously on the electrode [Eq. 1-7] (4,5).

$$CH_4 + CO_2 \leftrightarrow 2CO + 2H_2 \qquad \Delta H^o_{298} = 247 \text{ kJ mol}^{-1} \qquad [1]$$

$$CO_2 + H_2 \leftrightarrow CO + H_2O \qquad \Delta H^o_{298} = 41 \text{ kJ mol}^{-1} \qquad [2]$$

$$CH_4 \leftrightarrow C + 2H_2 \qquad \Delta H^o_{298} = 75 \text{ kJ mol}^{-1} \qquad [3]$$

The CO_2 reforming of methane (DRM) [Eq. 1] is a strongly endothermic process and therefore high temperatures (typically >750 ºC) are required to achieve high H_2 and CO

yields (6). Moreover, the catalytic Reverse Water Gas Shift (RWGS) reaction [Eq. 2] may run in parallel, resulting in the consumption of valuable H_2 and a decrease in H_2/CO ratio to values lower than unity (7). In addition, carbon deposition on the electrocatalyst surface due to CH_4 decomposition [Eq. 3] may also occur resulting in progressive electrocatalyst deactivation (8,9). The CH_4 decomposition [Eq. 3] is favoured at high temperatures (> 600 ^oC), whereas at temperatures below 650 ^oC carbon deposits are mainly produced by Boudouard reaction ($2CO \rightarrow C + CO_2$) (7-9). The H_2, CO and C produced, as well as the CH_4 supplied can be electrochemically oxidized by oxygen ions according to Eq. 4-7.

$$H_2 + O^{2-} \leftrightarrow H_2O + 2e^- \qquad \Delta H^o_{298} = -242 \text{ kJ mol}^{-1} \qquad [4]$$

$$CO + O^{2-} \leftrightarrow CO_2 + 2e^- \qquad \Delta H^o_{298} = -283 \text{ kJ mol}^{-1} \qquad [5]$$

$$CH_4 + O^{2-} \leftrightarrow CO + 2H_2 + 2e^- \qquad \Delta H^o_{298} = -37 \text{ kJ mol}^{-1} \qquad [6]$$

$$C(s) + O^{2-} \leftrightarrow CO + 2e^- \qquad \Delta H^o_{298} = -111 \text{ kJ mol}^{-1} \qquad [7]$$

Ni-based ceramic-metal composites with Yttria Stabilized Zirconia (YSZ) and Gadolinia Doped Ceria (GDC) are widely used as electrocatalysts in SOFCs because of their activity and inexpensiveness. According to the literature, Ni/GDC fuel electrodes show higher electrocatalytic activity for CH_4 reforming, resistance to carbon deposition, and tolerance levels for H_2S compared to Ni/YSZ electrodes (10,11). Authors attributed this behaviour to the capacity of CeO_2 to store and release oxygen, which favours the CH_4 oxidation and mitigates the carbon deposition (1,12). The carbon tolerance and anti-sintering tendency of nickel can be enhanced further, by dispersing trace amounts of transition noble (Rh, Pt, Pd, Ru, Au) or non-noble (Co, Cu, Mo, Fe) metal elements (3,13).

In this direction our research group with collaborators (2,3,13-17) attempted to study and modify commercial NiO/GDC powder with Au and/or Mo nanoparticles in solid oxide applications. These modifications resulted in electrocatalysts with high tolerance and improved electrocatalytic activity under oxidizing conditions (H_2O electrolysis) (16,17), carbon forming (Internal Steam Reforming of Methane, ISRM) and sulphur poisoning conditions (mixtures of H_2O/CH_4 including 10 ppm H_2S) (2,3,13-15). One of the main findings was the induced structural modification on nickel through the formation of bimetallic Au-Ni and ternary Au–Mo–Ni solid solutions. In these studies, using either helium diluted or non-dialuted harsh H_2O/CH_4 reaction mixtures, the main conclusion was that 3Au-0.4Mo-Ni/GDC proved to be the most carbon tolerant electrode, compared to Ni/GDC, 3Au-Ni/GDC and 0.4Mo-Ni/GDC. The superior performance of 3Au-0.4Mo-Ni/GDC was attributed to a synergistic interaction of Au-Mo-Ni that seems to protect nickel against carbon deposition (2,3,13-15). Although Au as a precious metal is expensive, its use may be justified if improved long term resistance to carbon is attained. The latter aspect can compensate the increase for the material's cost.

Iron is another metal, non precious, which has become a research hotspot due to its price advantage and it is suggested to improve electrocatalytic activity upon its addition on Ni-based electrocatalysts for reforming conditions (18-21). Our research group obtained also very interesting results by investigating the effect of Fe on Ni/GDC cermets for the solid oxide H_2O electrolysis reaction (22). The improved performance of modified nickel cermets with Fe has been attributed to the formation of a Fe-Ni alloy and to its improved redox properties (18,19,22). Recent studies related to DRM reaction over Fe-Ni/MgO catalysts (20) showed that Fe modification not only eliminates carbon deposition but it also

alters the nature of carbon towards a form that can be easily removed from the catalyst surface via gasification by CO_2.

In this study the performance of Ni/GDC, 3 wt.% Au-0.5 wt.% Fe-Ni/GDC and 3 wt.% Au-0.4 wt.% Mo-Ni/GDC electrodes was studied, at open circuit potential (OCP) and closed circuit potential (CCP) conditions, under biogas fuel operation in single SOFCs. Firstly, the electrodes were catalytically investigated, at 750-900 ºC, in the form of half-electrolyte supported cells (ESCs), under a mixture of CH_4/CO_2=1, in the presence of current collector. Then, the electrocatalysts were electrocatalytically investigated as fuel electrodes in full ESCs under similar conditions (i.e. temperature, mixture), versus various polarizations, in order to elucidate the modifying effect of 3 wt.% Au, 0.5 wt.% Fe and 0.4 wt.% Mo in Ni/GDC for IDRM operation.

Experimental

Preparation of powders and cells

The modified powders were prepared via the Deposition – Co Precipitation (D.CP.) method by using the commercial NiO/GDC cermet (65 wt.% NiO-35 wt.% GDC, Marion Technologies) as the support. The precursors for the 3 wt.% Au-0.5 wt.% Fe-NiO/GDC and 3 wt.% Au-0.4 wt.% Mo-NiO/GDC samples were $HAuCl_4$, $Fe(NO_3)_3x9H_2O$ and $(NH_4)_6Mo_7O_{24}$, purchased from Sigma-Aldrich. Full details about synthesis can be found elsewhere (14,22). After filtering, the precipitate was dried at 110 °C for 24 h and then each powder was calcined in air at 600 °C/ 90 min and a part of it at 1100 °C/75 min. In the following, the samples will be denoted as 3Au-0.5Fe-NiO/GDC and 3Au-0.4Mo-NiO/GDC.

The electrolyte-supported half and full cells consisted of a circular shaped planar 8YSZ electrolyte (by Kerafol) with 25 mm diameter and 300 μm thickness. As reported in a previous study (3), the deposition of the electrodes was made by using the screen-printing method and the paste which consisted of a proper amount of powder (calcined at 600 ºC), terpineol as the dispersant and PVB (polyvinylbutyral) as the binder, purchased from Sigma-Aldrich. After the paste-deposition, the cell was sintered at 1150 °C with a heating/cooling ramp rate of 2 °C/min. In the electrocatalytic experiments, the oxygen electrode was a porous $La_{0.6}Sr_{0.4}Co_{0.8}Fe_{0.2}O_{3-\delta}$ (LSCoF) (provided by SolydEra), which was also calcined at 1150 °C with the same ramp rate of 2 °C/min. In the oxygen side, an adhesion layer of GDC10 (10 mg cm^{-2}) was applied and pre-calcined at 1300 ºC for 2 h (rate: 2 °C/min), in order to overcome the thermal and chemical mismatch between LSCoF and YSZ electrolyte. The loadings of the examined fuel and oxygen electrodes were ~6 mg cm^{-2} and ~10 mg cm^{-2} respectively, with an active surface area of 1.8 cm^2, apart from 3Au-0.5Fe-NiO/GDC and 3Au-0.4Mo-NiO/GDC in the electrocatalytic measurements, which loading was ~12 mg cm^{-2}, whereas the loading of NiO/GDC was kept ~6 mg cm^{-2} in order to avoid technical problems due to carbon deposition.

Catalytic and electrocatalytic measurements

Originally, all the prepared fuel electrodes were catalytically investigated by applying a mixture of CH_4/CO_2=1, without dilution of the reactants in a carrier gas, at 750-900 ºC, in the form of half cells, including the presence of Ni mesh, in order to examine their performance without applying a current. The flow rate in the catalytic/kinetic experiments

varied between 150 and 300 cm^3/min. The findings from the catalytic investigation were used for the electrocatalytic measurements in full cells. The electrocatalytic experiments were carried out at 900 and 850 ºC, under the same mixture as that in catalytic measurements, through polarization curves (i-V) and subsequent electrochemical impedance spectroscopy (EIS). Specifically, the i-V data were recorded, by using an Autolab potentiostat/galvanonstat, (model PGSTAT30), between the open circuit potential and 0 V, at a scan rate of 5 mV s^{-1} and a step potential of 20 mV. The EIS were measured in galvanostatic mode at various current densities, with an amplitude of 20 mA, in the frequency range from 100 kHz to 20 mHz. As current collectors, Ni and Pt meshes were used on the fuel and oxygen side, respectively, and each electrocatalyst constituted the only functional layer of the fuel electrode, where the oxygen compartment was fed with 100 vol.% O_2. The flow rates in electrocatalytic measurements were adjusted at 50 cm^3/min in the fuel compartment and 100 cm^3/min in the oxygen compartment, in order to ensure the implementation of the cell testing without breaking it, due to non-dialuted harsh conditions. Reactants and products were determined, under OCP conditions as well as under various current densities, by using an on-line gas chromatograph (GC) (Varian CP-3800) with a thermal conductivity detector. A Porapak Q column (80–100 mesh, 1.8 m × 1/8 in. × 2 mm) was used for the analysis of H_2O at 150 ºC, while a Carbosieve S-11 column (80–100 mesh, 2 m × 1/8 in. × 2 mm) was used for the analysis of H_2, CO, CH_4 and CO_2 (in parallel with the Porapak Q).

Results and Discussion

Catalytic experiments on half cells were performed prior those of the full-electrolyte supported cells, in order to have a reference performance and coking resistance of each electrode under CO_2 reforming of CH_4 without the effect of the applied current. In regards to the "homogenous" catalytic production, no activity was observed. Concerning the current collector, Ni mesh, has shown low catalytic activity, under a mixture of CH_4/CO_2=50/50, towards the production of H_2, CO and H_2O. However, comparative measurements of Ni/GDC with and without the presence of Ni mesh (not shown here), suggest that there is no direct catalytic contribution of Ni mesh to the activity of the electrocatalysts.

Figures 1 and 2 show the catalytic performance of each electrode at 750-900 ºC, through the consumption/production rates of CH_4, CO_2, H_2, CO, H_2O and of the formed carbon and through the % conversions of CH_4 and CO_2, for the CO_2 reforming of CH_4 (CH_4/CO_2=50/50, $F_{tot,in}$=150 cm^3 min^{-1}). The measurements were performed on half cells that comprised only the electrocatalyst and Ni mesh. The catalytic rates of reactants and products were calculated through Eq. 8. Carbon cannot be detected by the GC, since it is deposited in solid form. Therefore, the calculation was carried out, by taking into account the consumption and production rates of the rest of the reactants and products (CH_4, CO_2, H_2, CO, H_2O). Hence, Eq. 9 was extracted from the combination of the mass balances of the DRM, RWGS and CH_4 decomposition reactions [Eq. 1-3], as similarly followed in another study of our research group for the CH_4 internal steam reforming reaction (3).

$$r_i \left[\frac{mol}{s}\right] = \frac{F\left[\frac{cm^3}{min}\right] * (C_{i,in} - C_{i,out})}{V_m * 60\left[\frac{s}{min}\right]} \quad [8]$$

where r_i is the consumption/production rate for H_2O, H_2, CO, CH_4 and CO_2, F is the total volumetric flow, V_m is the molecular volume of ideal gases (22,400 $\frac{cm^3}{mol}$), $C_{i,in}$ and $C_{i,out}$ $\left[\frac{cm^3}{min}\right]$ are the input/output concentrations of each compound respectively.

$$r_C = \frac{r_{H_2} + 2r_{H_2O} - r_{CO}}{2} \quad [9]$$

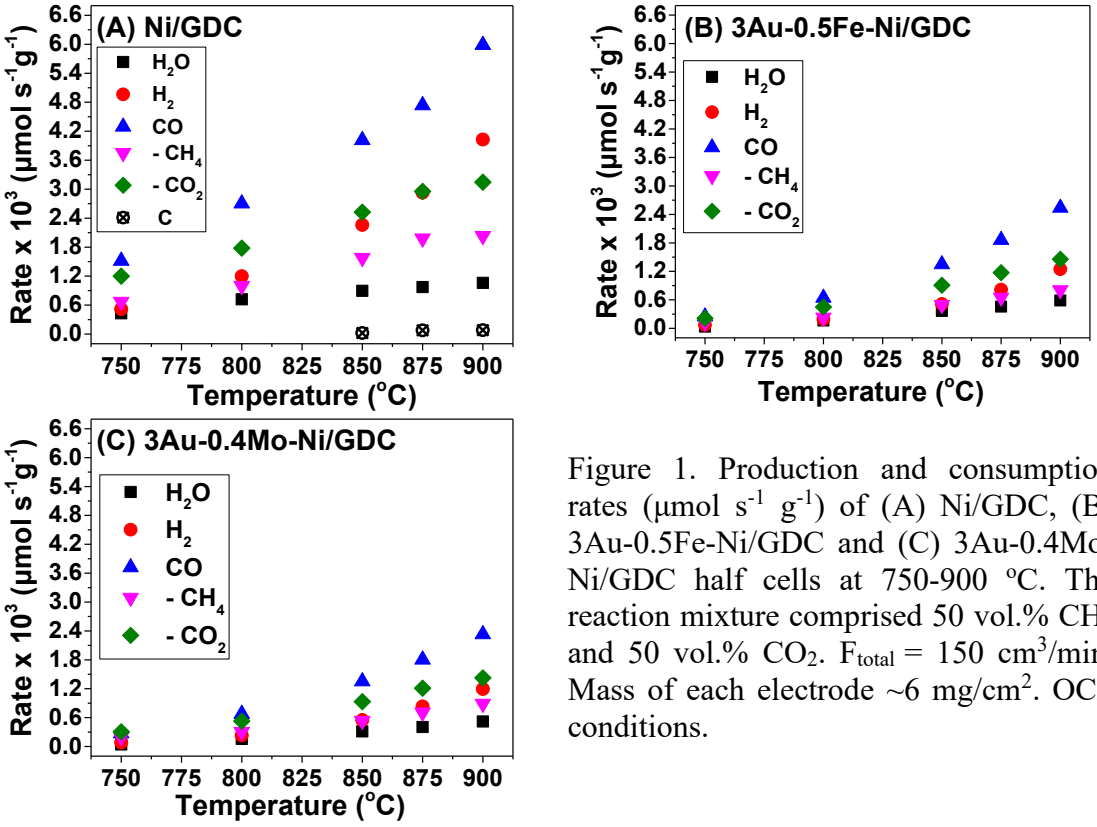

Figure 1. Production and consumption rates (µmol s^{-1} g^{-1}) of (A) Ni/GDC, (B) 3Au-0.5Fe-Ni/GDC and (C) 3Au-0.4Mo-Ni/GDC half cells at 750-900 °C. The reaction mixture comprised 50 vol.% CH_4 and 50 vol.% CO_2. F_{total} = 150 cm^3/min. Mass of each electrode ~6 mg/cm^2. OCP conditions.

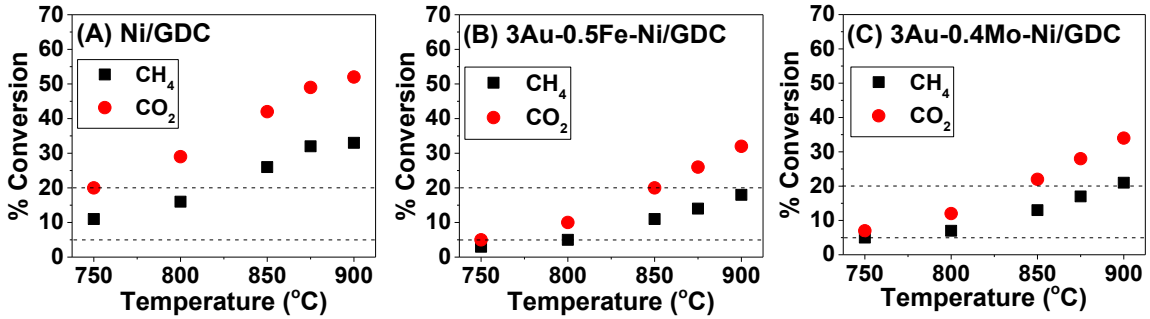

Figure 2. The corresponding % conversions of CH_4 and CO_2 of Fig. 1 for (A) Ni/GDC, (B) 3Au-0.5Fe-Ni/GDC and (C) 3Au-0.4Mo-Ni/GDC half cells at 750-900 °C. Mixt.: 50 vol.% CH_4–50 vol.% CO_2. F_{total} = 150 cm^3/min. Mass of each electrode ~6 mg/cm^2. OCP conditions. The dashed lines correspond to the differential conditions region.

Generally, it is observed that the % conversion of CO_2 was always higher than the % conversion of CH_4, due to the contribution of the RWGS reaction that consumes CO_2 and H_2 and resulted in a H_2/CO ratio less than unity. In respect to the catalytic performance, Ni/GDC was found to be the most active sample for the CO_2 reforming of CH_4 reaction,

yielding the highest consumption/production rates and % conversions. However, it exhibited carbon formation rates at high temperatures (≥850 °C), leading to fast deactivation. On the other hand, 3Au-0.5Fe-Ni/GDC and 3Au-0.4Mo-Ni/GDC were less active in terms of consumption/production rates and % conversions, but at the same time they were less prone to carbon formation.

The kinetic measurements were performed with gas flows in the range of 150-300 cm^3/min, where the reactor was operating under differential conditions with reactants' conversions between 5-20%. In the above gas flow range the reaction rates were found to remain practically constant, which corresponds to the absence of mass transfer limitations. Figure 3 presents the Arrhenius plots for the consumption rates of CH_4 and CO_2, under differential conditions, and the derived apparent activation energies ($E_{a,app}$) for each electrocatalyst. It is observed that the modified electrodes were less active for CH_4 and CO_2 consumption with relatively high $E_{a,app}$ values, compared to unmodified Ni/GDC. According to the literature (23), non-carbon forming CH_4 activation is the rate-determining step at high temperatures for both DRM and decomposition reactions. Furthermore, it is known that CH_4 is activated on metal surface sites (e.g. Ni), whereas CO_2 is mainly activated on support sites (e.g. GDC) in the vicinity of dispersed metal particles or/and on the metallic sites (7). The reported $E_{a,app}$ values, from other studies, for Ni-based catalysts vary in a wide range of 29-360 kJ/mol, which depends on the nature of the support, the presence of additives and the catalytic conditions (24). In the presented study the calculated $E_{a,app}$ for Ni/GDC is 63 kJ/mol for CH_4 activation, which coincides with the $E_{a,app}$ for CH_4 dissociation on Ni (1 1 0) and Ni (1 1 1) (25).

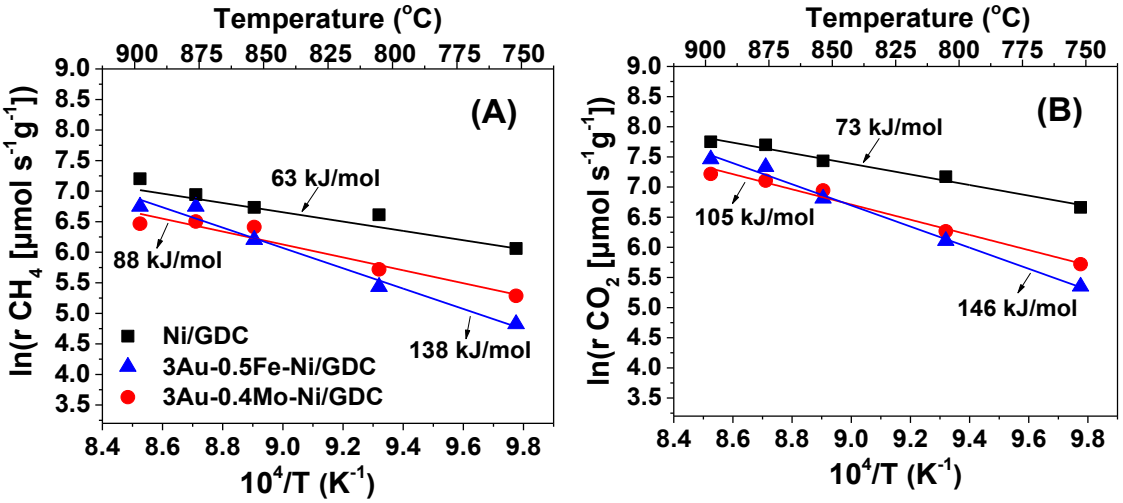

Figure 3. Arrhenius plots of the inherent consumption of (A) CH_4 and (B) CO_2 rates as a function of temperature (750-900 °C). The corresponding apparent activation energies ($E_{a,app}$, kJ/mol) are embedded. OCP and differential conditions under the mixture of 50 vol.% CH_4−50 vol.% CO_2. F_{total} is varied, 150-300 cm^3/min. Electrode mass ~6 mg/cm^2.

Overall, according to the catalytic measurements, the modified 3Au-0.5Fe-Ni/GDC and 3Au-0.4Mo-Ni/GDC electrodes were less active for H_2 and CO production, but at the same time were less prone to carbon formation, compared to Ni/GDC. Concerning the different pathways for activating CH_4, previous investigation from our research group on the kinetic performance of the Ni/GDC electrode under the internal CH_4 steam reforming process (2)

showed, in brief, that the conversion of CH_4 towards H_2 and CO proceeds mainly via a two-step mechanism:

$$CH_4 + S \leftrightarrow CH_2^* + H_2 \quad [10]$$

$$CH_2^* + H_2O \leftrightarrow CO + H_2 + S \quad [11]$$

where S denotes a vacant adsorption site for the dissociative adsorption of CH_4 and CH_2^* denotes the adsorbed methyl-species.

The Eq. 10 is considered to be mainly activated on nickel and leads to the formation of hydrogenated carbonaceous deposits (CH_2^*). The latter can be removed from the catalyst surface through the reaction with H_2O [Eq. 11], where this step in considered to be mainly activated on the reduced ceria sites and probably proceeds through the intermediate formation of low coverage adsorbed hydroxyl species. In this way, the rate determining step of the CH_4 reforming reaction on Ni/GDC is not the complete dehydrogenation of CH_4, but instead it is the H_2O assisted oxidative dissociation of methyl species CH_2^* into CO and H_2 (2). The latter approach is currently under thorough investigation for the DRM and the IDRM processes, focusing on the effect of CO_2 (in parallel to that of H_2O). Specifically, it is considered that further dehydrogenation of the CH_2^* species may be completely inhibited on 3Au-0.5Fe-Ni/GDC and 3Au-0.4Mo-Ni/GDC without affecting the reforming reaction rates significantly.

Figure 4 shows the characteristic i-V curves of the SOFCs comprising Ni/GDC, 3Au-0.5Fe-Ni/GDC and 3Au-0.4Mo-Ni/GDC as anodes, under a mixture of CH_4/CO_2=1, without dilution in a carrier gas, at 900 and 850 °C.

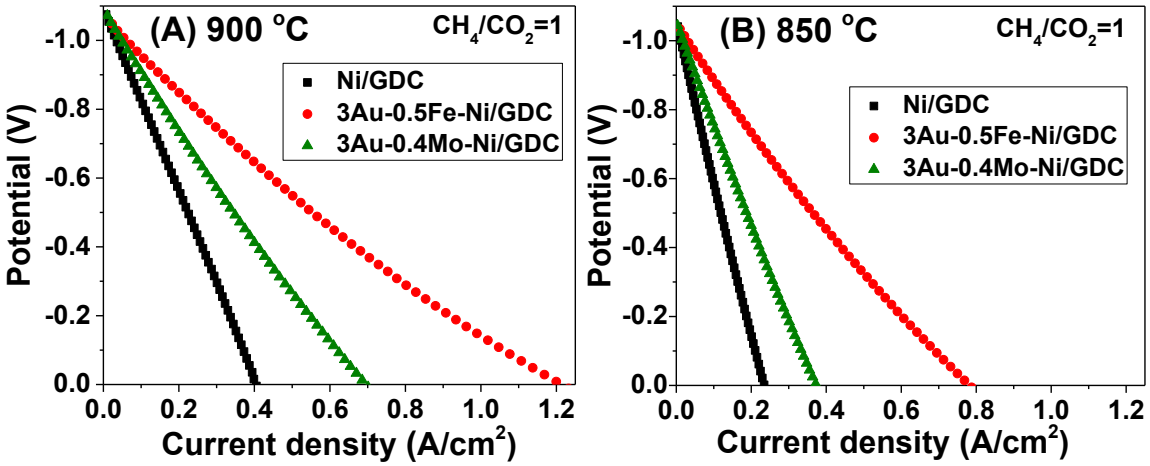

Figure 4. Polarization (i-V) curves at (A) 900 °C and (B) 850 °C for ESCs comprising Ni/GDC, 3Au-0.5Fe-Ni/GDC and 3Au-0.4Mo-Ni/GDC as fuel electrodes. IDRM conditions under a mixture of 50 vol.% CH_4–50 vol.% CO_2. $F_{total,\ in}$ = 50 cm^3/min.

Specifically, the cell with 3Au-0.5Fe-Ni/GDC exhibited the best performance, at both temperatures, since it provided in a wider range of current density at the same applied potential, compared to the other cells. In addition, the cell with 3Au-0.4Mo-Ni/GDC performed better than that with Ni/GDC, but worse than that with 3Au-0.5Fe-Ni/GDC. Another interesting observation is the effect of temperature on the performance, confirming

that the highest temperature promoted faster kinetics, which is reflected on the higher performance of the cells and the lower slopes in the i-V curves. It should be remarked that the cell with Ni/GDC exhibited the worst electrocatalytic performance for the IDRM process, compared to the cells with the modified electrodes, despite its higher DRM catalytic activity. This may be related to the different structural properties of Au-Mo and Au-Fe modified Ni/GDC electrodes. For this purpose, detailed physicochemical measurements are currently in progress, focusing on the changes of bulk and surface properties of the electrodes, by means of XRD, SEM and XPS measurements, which are the subject of a separate manuscript.

The effect of each modification on the ohmic and polarization characteristics of the cells, was further clarified and confirmed by means of EIS analysis. Specifically, in the Nyquist plots of Figure 5, R_{ohm} corresponds to the high frequency intersect on the real (Z') axis, while the low frequency intersect corresponds to the total resistance of the cell, R_t. R_t is the sum of ohmic and polarization resistances, $R_t = R_{ohm} + R_{pol}$, and by using this equation, the R_{pol} is obtained. Figure 5 exhibits the Nyquist plots for SOFCs comprising Ni/GDC, 3Au-0.5Fe-Ni/GDC and 3Au-0.4Mo-Ni/GDC as fuel electrodes, under the mixture of CH_4/CO_2=1, at 900 ºC, which were recorded under various applied current densities. The impedance spectra for cells with 3Au-0.5Fe-Ni/GDC and 3Au-0.4Mo-Ni/GDC were recorded in a wider range of applied current density values, compared to the cell with Ni/GDC, because the modified cells performed better. It should be mentioned that the highest applied current density value for each cell corresponded to a potential value close to ~0 V. The duration of each measurement and especially of that at ~0 V, was short ~10 min, in order to avoid the detrimental re-oxidation of the electrodes.

The first observation in Figure 5 shows that the cell with 3Au-0.5Fe-Ni/GDC exhibited the lowest R_{ohm} and R_{pol} values, compared to the other cells, which is another confirmation of its improved electrocatalytic performance. The cell with 3Au-0.4Mo-Ni/GDC showed higher R_{ohm} and R_{pol} values compared to that with 3Au-0.5Fe-Ni/GDC, which at the same time, were lower than that of the cell with Ni/GDC. It should be mentioned that R_{ohm} corresponds to the sum of the ohmic losses and comprises the contribution from the: (i) resistance of the connecting wires, (ii) the electronic resistance of the electrodes, particularly of the electrochemically inactive regions and most importantly (iii) the ionic resistance from the O^{2-} passage through the electrolyte. The fact that the modified cells exhibited lower R_{ohm} and R_{pol} values, compared to the unmodified, can be primarily ascribed to the higher electron conductivity and improved structural properties of the electrochemical interface between the ternary metal phases of Ni-Au-Fe or Ni-Au-Mo with GDC and the electrolyte. Previous findings from our research group (2, 13-17, 26, 27), highlight significant changes on the physicochemical and electrochemical properties of the Mo/Au-modified electrodes. In this respect, one explanation for the variation in the R_{ohm} and R_{pol} values deals with the connectivity of the Ni particles, which are the main pathway for the transfer of electrons. The reported (16,17) interaction of Ni-Au-Mo, may modify the surface energy and/or surface tension of the Ni particles and their interfacial surface with GDC. This change may result in a more stable structure and better connectivity of the Ni network, which is shown on the decreased R_{ohm} values of the H_2-reduced ternary electrodes. The above observation is currently under further investigation in order to clarify the reasons for the superior performance of 3Au-0.4Mo-Ni/GDC and especially for 3Au-0.5Fe-Ni/GDC and to understand the induced structural modifications, as well as the

subsequent effect on the electrocatalytic properties. The detailed interpretation of these measurements is the subject of a separate manuscript.

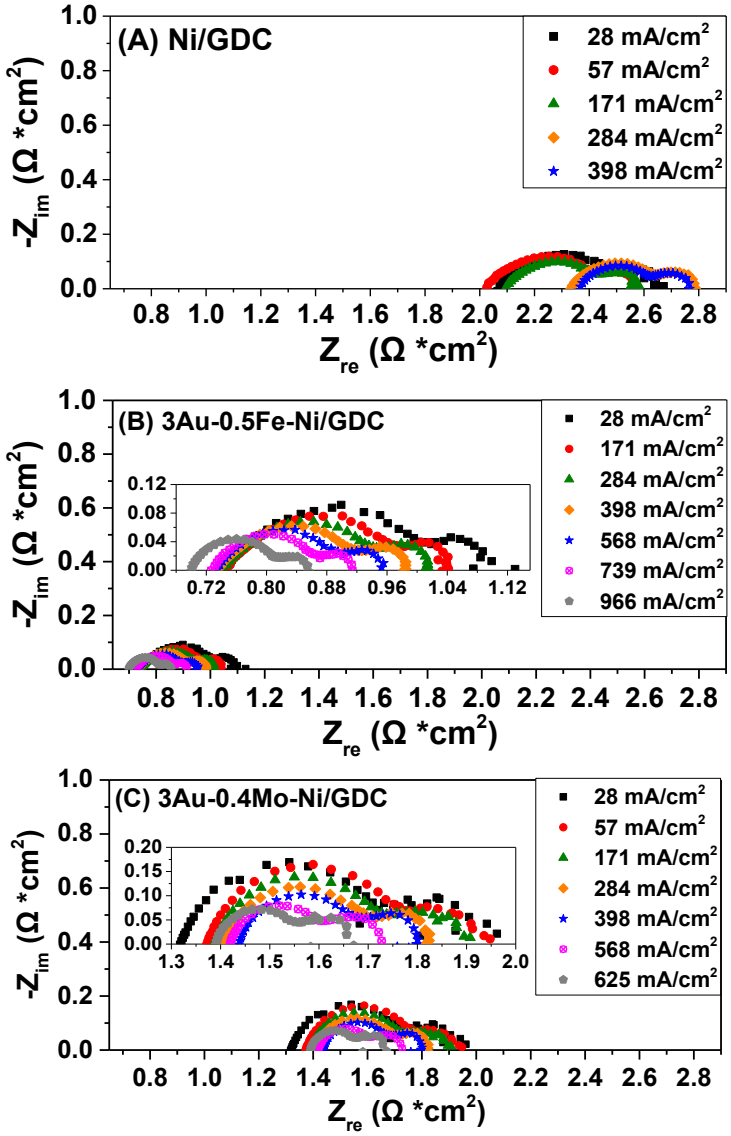

Figure 5. EIS measurements (Nyquist plots) of ESCs comprising (A) Ni/GDC, (B) 3Au-0.5Fe-Ni/GDC and (C) 3Au-0.4Mo-Ni/GDC as fuel electrodes, at 900 ºC, under various polarizations (applied current, mA cm^{-2}). Mixt.: 50 vol.% CH_4–50 vol.% CO_2. $F_{total,\ in}$ = 50 cm^3/min. Magnification figures of (B) and (C) plots are also shown inside the corresponding graphs.

Furthermore, by increasing the applied current density values for all cells there was a gradual decrease on the polarization characteristics (R_{pol} values), implying improved charge transfer and electrode processes (3,16,17). On the contrary, the most obvious differences between the cells, that caused the increase of polarization, are observed in the ohmic characteristics. Specifically, for the cell with Ni/GDC the increase of the applied polarization resulted in the deterioration (increase) of R_{ohm} value, due to possible gradual re-oxidation of the Ni/GDC electrode. On the other hand, in the case of the cells with the modified electrodes the R_{ohm} value was the least affected. Interestingly, the R_{ohm} value for the cell with 3Au-0.5Fe-Ni/GDC remained practically the same, by increasing the applied

polarization, while the R_{ohm} for the cell with 3Au-0.4Mo-Ni/GDC was slightly increased. Another observation is the decreased R_{ohm} and R_{pol} values in the case of the cell with 3Au-0.5Fe-Ni/GDC, under the highest polarization of 966 mA cm^{-2}, indicating the improvement of its performance.

The outlet gas from the fuel side compartment was also analyzed under fuel cell conditions through GC measurements to evaluate any changes in the reactants/products, compared to the open circuit potential conditions. Figure 6 exhibits the electrocatalytic performance of each electrode, at 900 ºC, through the consumption/production rates of CH_4, CO_2, H_2, CO and H_2O for the internal CO_2 reforming of CH_4 (CH_4/CO_2=50/50, $F_{tot,in}$=50 cm^3/min). The carbon formation rates were calculated, like in the half cell measurements, by using the following mass balance expression of carbon [Eq. 12]. The calculation was accomplished, by taking into account the carbon mass balance under catalytic conditions [Eq. 9], the changes in the production rates (Δr_i) of i= CO_2, CO, H_2O and H_2 due to the applied polarization [Eq. 13] and the faradaic rate of the electrochemical O^{2-} flux ($r_{O^{2-}}$) [Eq. 14]. Thus, Eq. 14 was extracted from the combination of the mass balances of the catalytic and electrocatalytic reactions, for IDRM [Eq. 1-6]. This expression is valid under both open circuit potential and fuel cell conditions.

$$r_C = \frac{r_{H_2} + 2r_{H_2O} - r_{CO} - \frac{I}{nF}}{2} \quad [12]$$

where: r (mol s^{-1}), I (A) is the applied current, n = 2 is the number of the participating electrons and F is the Faraday constant (96,485 Cb mol^{-1}).

$$\Delta r_i = r_{i,polarization} - r_{i,ocp} \quad [13]$$

where: $r_{i,polarization}$ (mol s^{-1}) is the rate of CO_2, H_2, CO or H_2O under fuel cell conditions and $r_{i,ocp}$ (mol s^{-1}) is the corresponding rate of each compound under catalytic conditions.

$$r_{O^{2-}} = \frac{I}{nF} \quad [14]$$

Regarding the effect of polarization on the production rates of H_2 and CO, it is observed that the increase of polarization resulted in increased r_{H2} and r_{CO} in the case of Ni/GDC, whereas for the cases of 3Au-0.5Fe-Ni/GDC and 3Au-0.4Mo-Ni/GDC the corresponding rates decreased. High polarization caused also an increase in the production rate of H_2O. However, the modified electrodes did not favor the production of H_2O, compared to Ni/GDC, by applying the same current density values (i.e. up to 400 mA cm^{-2}). Moreover, Ni/GDC exhibited higher rates, compared to the modified electrodes, though the latter achieved higher current densities under the same applied potential. This is attributed to the higher catalytic activity of Ni/GDC for the DRM reaction, as already detected in the half cell (OCP) measurements. The 3Au-0.5Fe-Ni/GDC and 3Au-0.4Mo-Ni/GDC cells were less active.

Nevertheless, despite the lower production rates of H_2 and CO, these seem to be more than enough for the modified cells to operate electrochemically better, as also reported (3) in the case of the internal CH_4 steam reforming reaction. Furthermore, the presence of oxygen ions in the reactive environment, under fuel cell conditions, seems to effectively

suppress carbon deposits [Fig. 6]. As already reported (10) under fuel cell conditions the O^{2-} ions, which are transferred through the electrolyte to the fuel side, can easily oxidize the adsorbed carbon according to Eq. 7. However, the removal of the formed carbon is mainly located to the triple-phase boundary zone and thus degradation due to cumulative carbon deposition may be present, especially during prolonged operation.

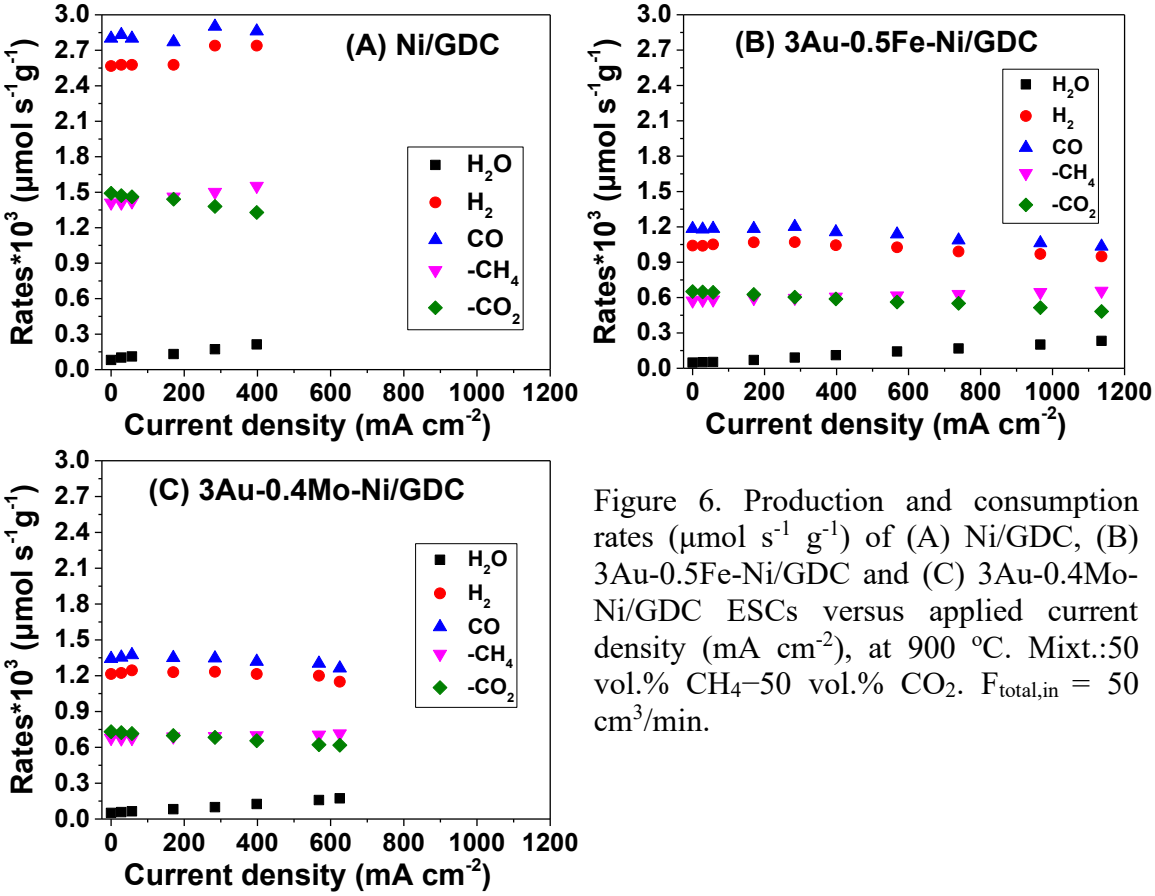

Figure 6. Production and consumption rates (μmol s^{-1} g^{-1}) of (A) Ni/GDC, (B) 3Au-0.5Fe-Ni/GDC and (C) 3Au-0.4Mo-Ni/GDC ESCs versus applied current density (mA cm^{-2}), at 900 ºC. Mixt.:50 vol.% CH_4–50 vol.% CO_2. $F_{total,in}$ = 50 cm^3/min.

Further electrocatalytic and physicochemical measurements are currently in progress, in an attempt to study the effect of Fe-Au modification on the CH_4 dehydrogenation routes under IDRM conditions. The aim is to decrease the Au wt.% content and optimize the electrocatalytic performance, as well as to perform stability measurements.

Conclusions

In respect to the open circuit catalytic performance, Ni/GDC was found to be the most active electrode for the CO_2 reforming of CH_4 reaction, yielding the highest consumption/production rates and % conversions. However, it exhibited carbon formation rates at high temperatures (≥850 ºC), leading to fast deactivation. On the other hand, 3Au-0.5Fe-Ni/GDC and 3Au-0.4Mo-Ni/GDC electrodes were less active in terms of consumption/production rates and % conversions, but at the same time were less prone to carbon formation.

Regarding the electrocatalytic performance, the cell with 3Au-0.5Fe-Ni/GDC exhibited the highest activity, at 900 and 850 ºC, since it operated in a wider range of current density, whereas it exhibited the lowest R_{ohm} and R_{pol} values, compared to the other examined cells. The cell with 3Au-0.4Mo-Ni/GDC performed better than Ni/GDC, but worse than that with

3Au-0.5Fe-Ni/GDC. Furthermore, the increase of polarization resulted in the deterioration of R_{ohm} for the cell with Ni/GDC, whereas for the cells with the modified electrodes R_{ohm} was the least affected. Moreover, under fuel cell operation, the presence of O^{2-}, seems to suppress carbon deposits. In addition, the increase of polarization caused an increase of r_{H2} and r_{CO} for the cell with Ni/GDC, whereas for the cells with 3Au-0.5Fe-Ni/GDC and 3Au-0.4Mo-Ni/GDC the corresponding rates decreased and this is under further evaluation. Finally, the modified electrodes did not favor the production of H_2O through the RWGS, which is considered as beneficial for the selectivity of the electrocatalysts to the desired fuels for the cells' operation.

Acknowledgments

This research has been co-financed by the European Union and Greek national funds through the operational program *'Regional Excellence'* and the operational program *'Competitiveness, Entrepreneurship and Innovation'*, under the call "**RESEARCH-CREATE-INNOVATE**" (Project code: **T2EΔK-00955**).

References

1. M.J. Escudero, C.A. Maffiotte and J.L. Serrano, *J. Power Sources,* **481**, 229048 (2021).
2. S. Souentie, M. Athanasiou, D.K. Niakolas, A. Katsaounis, S.G. Neophytides and C.G. Vayenas, *J. Catal.*, **306**, 116-128 (2013).
3. Ch. Neofytidis, V. Dracopoulos, S.G. Neophytides and D.K. Niakolas, *Catal. Tod.,* **310**, 157-165 (2018).
4. M.J. Escudero and J.L. Serrano, *Int. J. Hydrogen En.,* **44** (36) 20616-20631 (2019).
5. M. Chlipałaa, P. Błaszczaka, S.F. Wang and B. Bochentyna, *Int. J. Hydrogen En.,* **44** (26) 13864-13874 (2019).
6. N.A.K. Aramouni, J.G. Touma, B.A. Tarbousha, J. Zeaitera and M.N. Ahmad, *Renewable and Sust. Energy Rev.* **82**, 2570-2585 (2018).
7. I.V. Yentekakis, P. Panagiotopoulou and G. Artemakis, *Applied Cat. B.: Environ.,* **296**, 120210 (2021).
8. D. Pakhare and J. Spivey, *Chem. Soc. Rev.,* **43**, 7813-7837 (2014).
9. M.K. Nikoo and N.A.S. Amin, *Fuel Process. Technol.,* **92**, 678-691 (2011).
10. M.A. Abdelkareem, W.H. Tanveer and E.T. Sayed, *Renew. Sustain. Ener. Rev.,* **101**, 361-375 (2019).
11. W. Wang, C. Su, Y. Wu, R. Ran and Z. Shao, *Chem. Rev.,* **113**, 8104-8151 (2013).
12. N. Mahato, A. Banerjee, A. Gupta, S. Omar and K. Balania, *Prog. Mater. Sci.,* **72**, 141-337 (2015).
13. D.K. Niakolas, J.P. Ouweltjes, G. Rietveld, V. Dracopoulos and S.G. Neophytides, *Int. J. Hydrogen En.,* **35**, 7898-1904 (2010).
14. D.K. Niakolas, M. Athanasiou, V. Dracopoulos, I. Tsiaoussis, S. Bebelis and S.G. Neophytides, *Appl. Cat. A.: Gen.,* **456**, 223-232 (2013).
15. D.K. Niakolas, Ch. Neofytidis and S.G. Neophytides, S.G. *Frontiers in Environ. Science,* **5**, 78 (2017).
16. E. Ioannidou, Ch. Neofytidis, L. Sygellou and D.K. Niakolas, *Appl. Cat. B.: Environ.,* **236**, 253-264 (2018).
17. Ch. Neofytidis, E. Ioannidou, L. Sygellou, M. Kollia and D.K. Niakolas, *J. Catal.,* **373**, 260-275 (2019).

18. H. Kan and H. Lee, *Cat. Communications,* **12**, 36-39 (2010).
19. S.A. Theofanidis, V.V. Galvita, H. Poelman and G.B. Marin, *ACS Catal.,* **5**, 3028-3039 (2015).
20. T. Zhang, Z. Liu, Y.A. Zhu and Z. Liu, *Appl. Cat. B: Environ.*, **264**, 118497 (2020).
21. S. Joo, A. Seong, O. Kwon and K. Kim, *Sci. Adv.,* **6** (35), 1573 (2020).
22. Ch. Neofytidis, E. Ioannidou, M. Kollia, S.G. Neophytides and D.K. Niakolas, *Int. J. Energy Res.,* **44** (13), 10982-10995 (2020).
23. A. Kambolis, H. Matralis, A. Trovarelli and C. Papadopoulou, *Appl. Catal. A Gen.*, **377** (1–2), 16-26 (2010).
24. M.C.J. Bradford and M.A. Vannice, *Catal. Rev. - Sci. Eng.*, **41** (1), 1-42 (1999).
25. I. Luisetto, S. Tuti, C. Romano, M. Boaro and E. Di Bartolomeo, *J. CO2 Util.,* **30**, 63-78 (2019).
26. C. Neofytidis, M. Athanasiou, S.G. Neophytides and D.K. Niakolas, *Top. in Catal.*, **58** 1276-1289 (2015).
27. D.K. Niakolas, *Appl. Catal. A: Gen.*, **486** 123-142 (2014).